



## Ar-implantation on AISI 304 stainless steel against pit initiation processes

L. Martinez, Brahim Malki, Grégory Berthomé, Bernard Baroux, Francisco Javier Pérez-Trujillo

### ► To cite this version:

L. Martinez, Brahim Malki, Grégory Berthomé, Bernard Baroux, Francisco Javier Pérez-Trujillo. Ar-implantation on AISI 304 stainless steel against pit initiation processes. *Surface and Coatings Technology*, 2006, 201 (3-4), pp.1671-1678. 10.1016/j.surfcoat.2006.02.042 . hal-00140856

**HAL Id: hal-00140856**

**<https://hal.science/hal-00140856>**

Submitted on 16 Sep 2022

**HAL** is a multi-disciplinary open access archive for the deposit and dissemination of scientific research documents, whether they are published or not. The documents may come from teaching and research institutions in France or abroad, or from public or private research centers.

L'archive ouverte pluridisciplinaire **HAL**, est destinée au dépôt et à la diffusion de documents scientifiques de niveau recherche, publiés ou non, émanant des établissements d'enseignement et de recherche français ou étrangers, des laboratoires publics ou privés.



Distributed under a Creative Commons Attribution - NonCommercial 4.0 International License

# Ar-implantation on AISI 304 stainless steel against pit initiation processes

L. Martínez <sup>a</sup>, B. Malki <sup>b</sup>, G. Berthomé <sup>b</sup>, B. Baroux <sup>b</sup>, F.J. Pérez <sup>a,\*</sup>

<sup>a</sup> *Universidad Complutense de Madrid, Departamento de Ciencia de los Materiales e Ingeniería Metalúrgica, 28040 Madrid, Spain*

<sup>b</sup> *LTPCM-INPG Institute National Polytechnique de Grenoble, St Martin d'Hères 38402, France*

Ion implantation has been widely used as a surface modification technique to improve surface properties. However, a few works have been performed using argon as implanted element in order to modify the corrosion behaviour of stainless steels (SS). In the present study, the implanted ion was Ar<sup>+</sup> at an energy of 80 keV and the implanted dose was in the range of  $1 \times 10^{15}$  to  $1 \times 10^{17}$  Ar<sup>+</sup>/cm<sup>2</sup> in an AISI 304 stainless steel. The surface bombardment with inert gases mainly produces structural changes, modifying topography and morphology. Nevertheless, the surface analysis carried out by X-ray Photoelectron Spectroscopy (XPS) shows that Ar-implantation modifies the surface composition of the passive layer and, therefore, the protective properties of the SS. In order to measure these modifications on the corrosion behaviour, electrochemical noise tests at open circuit potential were performed. The results obtained show that Ar-implantation decrease the corrosion resistance of AISI 304 SS and this effect is more important with the increasing implantation dose.

**Keywords:** Ion implantation; Surface modification; Stainless steel

## 1. Introduction

The corrosion resistance is closely related to the composition and structure of surface films on metals as well as environmental factors [1,2]. Some advantages of ion implantation in regard to corrosion prevention are that special alloys can be obtained at the surface of a metal or alloy without alteration or sacrifice of bulk properties [1], that achieve unique properties that standard metallurgical treatments cannot bring out [3]. This technique has the advantage that it can be controlled accurately [4] and is particularly useful when the dimensions of the treated piece cannot be modified: for instance, in bearings or body implants [5–7].

Apart from the chemical modifications, microstructural defects due to the interaction between the ions of the ion beam and the host atoms are produced, which modify the corrosion resistance [5]. In order to study the balance between chemical effects induced by the nature of the implanted ion and the physical effects induced by the implantation process, inert gases can be implanted [8]. However, only a few works have

been performed using inert gases as an implanted element [8,9]. The surface bombardment with inert gases ions mainly produces structural changes, modifies the topography and morphology, but also introduces chemical changes on the surface sample [10].

The study of the localised corrosion phenomena in a non-potentiostatic way is particularly useful in finding out the early stages of the pitting process. One of the possibilities in this kind of studies is the electrochemical noise measured at the open circuit potential (OCP). With this technique, two identical freely corroding electrodes are located face to face and the fluctuations in potential (smaller than mV) and current (lower than  $\mu$ A) between them are measured. The analysis of these fluctuations provides information concerning the early stages of the pitting process. Current fluctuations reflect metal dissolution and indicate the corrosion intensity. At the same time, equivalent potential fluctuations take place and provide information about the metal–solution interface [11]. Small current transients corresponding to localised breakdown events can be detected at potentials below the stable pitting potential [12].

The aim of this work is to study the early stages of the pitting process on Ar-implanted AISI 304 SS. Previous studies concerning the corrosion behaviour of Ar-implanted AISI 304 SS

\* Corresponding author. Tel.: +34 91 394 4215; fax: +34 91 394 4357.

E-mail address: fjperez@quim.ucm.es (F.J. Pérez).

performed with Electrochemical Impedance Spectroscopy (EIS) showed certain improvement on the protective properties [13].

## 2. Experimental procedure

A commercial austenitic AISI 304 SS having the composition (wt.%): 0.44 Si, 1.52 Mn, 8.19 Ni, 0.29 Cu, 18.30 Cr, 0.031 P, 0.21 Mo, 0.12 Co, 0.065 C, 0.002 S, 0.038 N, 0.013 Sn, was used in the present study. The  $1 \times 1 \times 0.2$  cm<sup>2</sup> specimens were polished with SiC #600 emery paper and implanted with  $1 \times 10^{15}$ ,  $1 \times 10^{16}$  and  $1 \times 10^{17}$  Ar<sup>+</sup>/cm<sup>2</sup> at 80 keV. Argon ions (Ar<sup>+</sup>) were obtained from a Penning ion source, with a maximum acceleration tension of 300 kV. The ion beam current density was 400 nA/cm<sup>2</sup> and the implantation lasted for 2 h. A diffusion pump generated a vacuum of  $1.3 \times 10^{-5}$  Pa in the chamber. The acceleration chamber was equipped with a rotating circular holder of 9 cm diameter. Theoretical simulations of the implantation process have been performed with the SRIM 2003 computational code for 100,000 ions [14]. For surface

characterisation, X-ray Photoelectron Spectroscopy (XPS) studies were carried out before the electrochemical tests. The samples were cleaned with distilled water, acetone and distilled water again before putting them in a plasma chamber at 50 W and 1 Torr for 3 min in order to remove the contamination layer. The XPS studies were carried out in an electron spectrometer XR3E2 of Vacuum Generators with a Mg K $\alpha$  X-ray source ( $h\nu = 1253.6$  eV). After a general spectrum acquisition, the binding energy (BE) scale was calibrated using Au. Different spectra were taken for the energies corresponding to the core levels: Fe 2p<sub>3/2</sub>, Cr 2p<sub>3/2</sub>, O 1s<sub>1/2</sub> and Ar 2p<sub>3/2</sub>. This equipment has the ability to modify the angle involving the analyser and the surface sample between 90° and 30°, allowing the analysis of different depths in a non-destructive way depending on the angle employed. In the case of stainless steels, these penetration depths correspond approximately to the oxide layer, in the case of 30°, and the metal matrix, in the case of 90°. The Spectrum–Imagum software of R&D International was used for the acquisition and analysis of the XPS spectra.

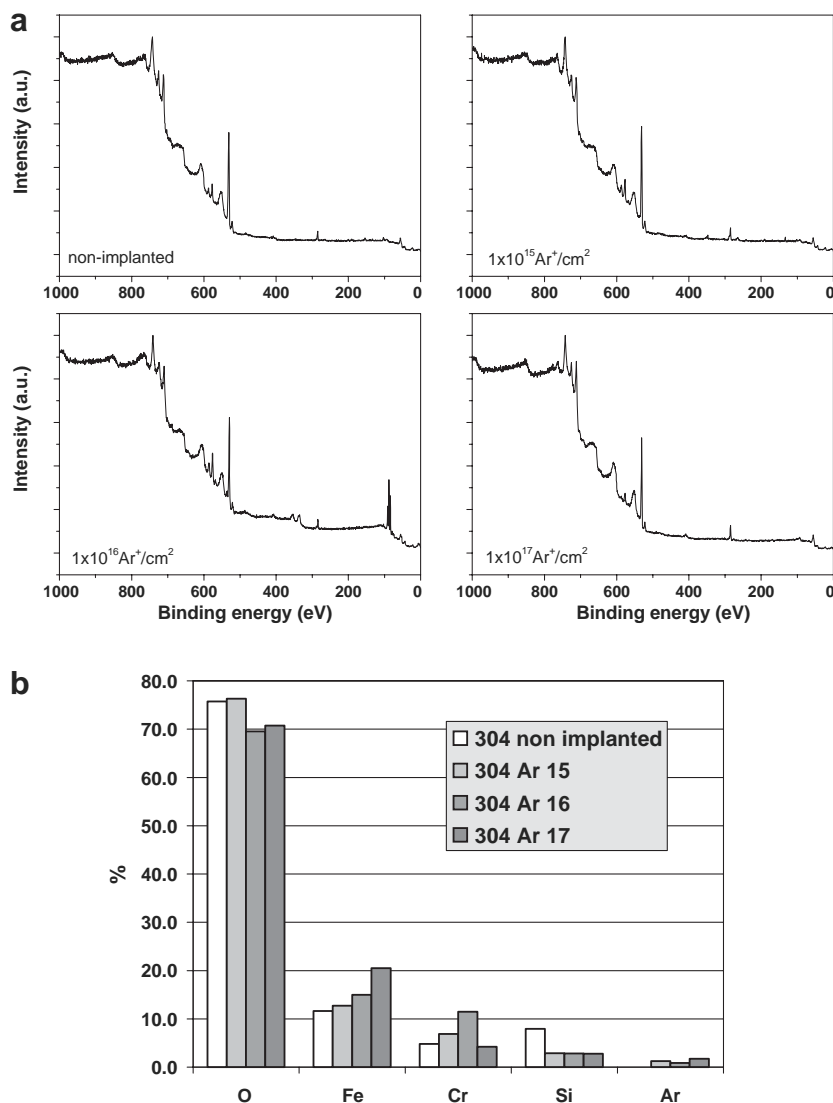


Fig. 1. (a) XPS general spectra of all the tested samples. (b) Relative percentage of the main alloying elements (without carbon) of AISI 304 SS at a take off angle of 90° with the different Ar-implantation doses.

The electrochemical tests were carried out at the OCP by using an Alpes Instruments controlled by the Mustig program described elsewhere [15]. These kinds of experiments measure the fluctuation in potential and intensity of two identical samples without any polarization. The samples were immersed for 24 h in a 1 M NaCl solution at room temperature and a pH=6.6 in order to obtain enough stability between electrode and electrolyte. After this period, a strong oxidising solution such as  $2 \times 10^{-4}$  M  $\text{FeCl}_3$  was added to ensure the appearance of pits in the system at pH=3.5 for another 24 h.

### 3. Results and discussion

The simulation of the implantation process performed with TRIM 2003 computational code resulted in a projected range and straggle:  $\text{RP} \pm \Delta\text{RP} = 36.3 \pm 15.2$  nm. The combination of the  $\text{Ar}^+$  mass and the energy employed in the process resulted in an argon distribution close to the surface with a small straggle ( $\Delta\text{RP}$ ). As a consequence, an important number of collisions and atom displacements occurred to obtain such ion distribution. As an approximation, around 0.22 collisions/ion/nm took place and produced a damaged region in the outermost part of the metal surface that will play an important role on the material's behaviour.

Figs. 1–6 show the XPS results of the Ar-implanted AISI 304 SS. Angle dependent XPS studies were performed at  $90^\circ$  and  $30^\circ$  in the Ar-implanted and non-implanted AISI 304 SS to find out whether Ar-implantation modified the relation between the main elements responsible for the protective properties of the passive layer (Fe, Cr and O) and to obtain additional information about the thickness of the passive layer [16]. Fig. 1a shows the general XPS spectra of all the tested samples. From

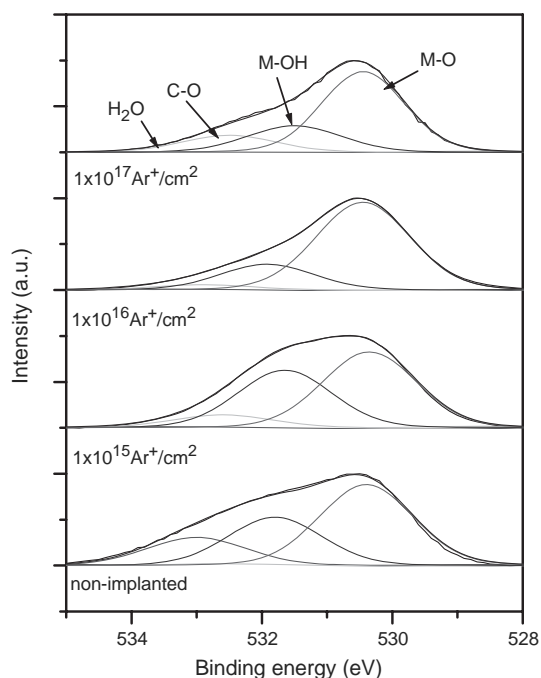


Fig. 2. Deconvolution of the O  $1s_{1/2}$  peak on the analysis at  $90^\circ$  of the Ar-implanted AISI 304 SS.

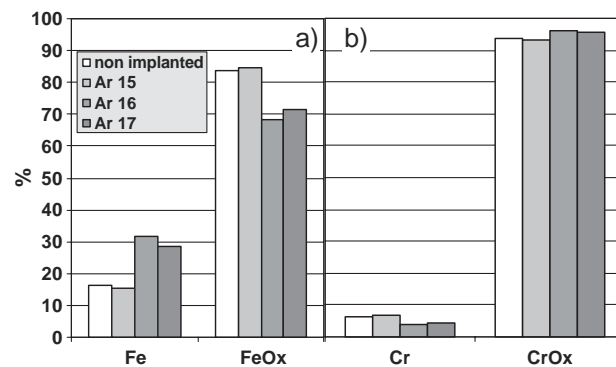


Fig. 3. Analysis of the (a) Fe  $2p_{3/2}$  and (b) Cr  $2p_{3/2}$  peaks at a take off angle of  $90^\circ$  of the Ar-implanted AISI 304 SS.

these plots can be derived the relative percentage of the main alloying elements responsible for the protective properties of the passive layer in the deeper analysis at  $90^\circ$  (Fig. 1b). Ar-implantation produced significant differences in the surface composition of AISI 304 SS and only the  $1 \times 10^{15} \text{ Ar}^+/\text{cm}^2$  dose presented a similar composition to the non-implanted SS. Higher implantation doses ( $1 \times 10^{16}$  and  $1 \times 10^{17} \text{ Ar}^+/\text{cm}^2$ ) decreased the relative oxygen content and increased the relative amount of iron in AISI 304 SS. The highest  $1 \times 10^{17} \text{ Ar}^+/\text{cm}^2$  dose presented the biggest modifications of the surface composition with an important Cr reduction, the main constituent of the protective passive film. On the other hand, Ar-implantation drastically reduced the Si peak into a nearly constant value independent of the implantation dose. Silicon is a characteristic element of the external part of the passive layer in contact with the solution due to its avidity for O [2] and Ar bombardment seems to remove it from the surface. During ion implantation, certain sputtering takes place no matter how small the ion dose is. Nevertheless, these effects are considered negligible for ion doses below  $10^{15} \text{ Ar}^+/\text{cm}^2$  [17]. Fig. 1b also showed the presence of around 1.5% Ar in all the implanted samples. Ar is an inert gas which does not combine with any other element in the SS but remained inside the structure. Other studies using He [18] and Xe [19] ion implantation into stainless steels found that the inert gases agglomerates in form of gas bubbles. This effect was not studied in this work, although the presence of gas atoms

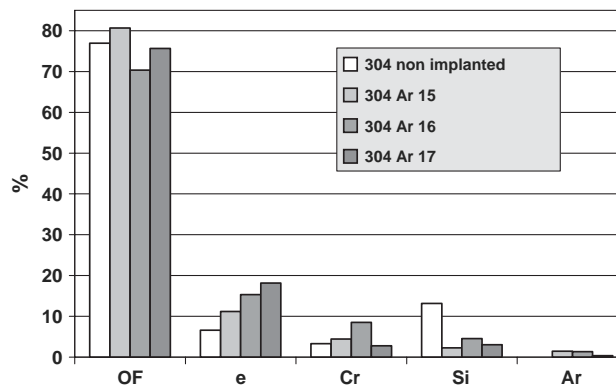


Fig. 4. Relative percentage of the main alloying elements (without carbon) of AISI 304 SS at a take off angle of  $90^\circ$  with the different Ar-implantation doses.

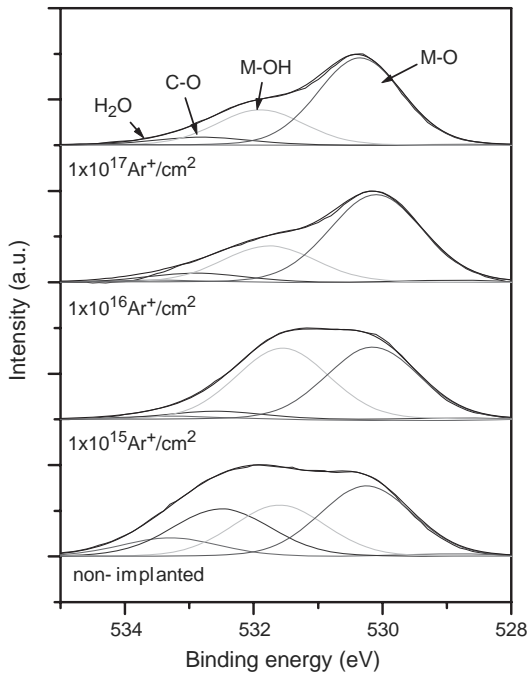


Fig. 5. Deconvolution of the O  $1s_{1/2}$  peak on the analysis at  $30^\circ$  of the Ar-implanted AISI 304 SS.

trapped inside the SS generates strong residual stresses due to the volume ratio and conditioned the material's behaviour.

Fig. 2 shows a comparison of the O  $1s_{1/2}$  peak. In all cases, the metal– oxygen (M-O, BE=530.1 eV) bonding was more abundant than the metal–hydroxide (M-OH, BE=531.5 eV) one. Only the  $10^{15}$  Ar $^+$ /cm $^2$  dose increased the amount of M-OH on AISI 304 SS, while higher implantation doses reduced this component. Generally, the passive layer of SS is presented as an inner layer mainly composed of chromium oxide, and an external layer composed of iron oxides and hydroxides [20,21]. The decrease in the M-OH and C–O components – this last one related to the contamination layer – with the previously mentioned decrease in Si suggested a partial destruction of the outer region of the passive layer due to sputtering with Ar-implantation [11] for doses higher than  $10^{16}$  Ar $^+$ /cm $^2$ .

In order to confirm this fact, Fig. 3 shows the proportion of metallic and oxidised metal derived from the deconvolution of the Fe  $2p_{3/2}$  (a) and Cr  $2p_{3/2}$  (b) peaks. Fig. 3a shows the analysis of the Fe  $2p_{3/2}$  peak. A decrease in the amount of Fe joined with oxygen (Fe-Ox) in favour to the metallic component was observed on the higher implantation doses, that supported the existence of certain sputtering. In contrast, smaller variations were found in the analysis of the Cr  $2p_{3/2}$  spectrum (Fig. 3b), where just a slight increase on the Cr-Ox from 94% of the non-implanted to 96% of the highest implantation dose was found. This fact was also in accordance to the removal of the outer Fe-rich region of the passive layer and the inner region remained with small modifications.

Differences between the Fe and Cr bonding with oxygen were not distinguished in the deconvolution of the correspondent Fe and Cr spectra due to the energy proximity of the different components and the formation of non-stoichiometric

compounds associated to the ion implantation process. The BE of the Fe peak (between 710.9 and 711.3 eV) suggested an important contribution of FeOOH in all samples, whereas in the case of Cr, the BE shifted from 577 eV of the non-implanted sample corresponding to Cr(OH) $_3$  to 576.8–576.9 eV of the implanted samples, suggested the formation of intermediate compounds between Cr $_2$ O $_3$  and Cr(OH) $_3$ . Therefore, Ar-implantation proportioned better chemical conditions, in terms of corrosion protection, to AISI 304 SS due to the higher contribution of the protective Cr $_2$ O $_3$  component on the implanted samples.

Fig. 4 compare the relative percentage of the main alloying elements responsible for the protective properties of the passive layer in a more superficial study at  $30^\circ$ . A constant Fe and Cr increase was observed with the increasing implantation dose on the external region of the passive film, except for a Cr decrease in the  $10^{17}$  Ar $^+$ /cm $^2$  dose. In this analysis, no metallic component was neither expected nor found and the contributions of Fe and Cr are all due to the oxidised form. A decrease of the binding energy by 0.3 eV suggested a higher contribution of the oxide form, especially in the Cr peak. Only the lower implantation dose ( $10^{15}$  Ar $^+$ /cm $^2$ ) increased the relative oxygen content on the surface of AISI 304 SS. In this superficial analysis, the decrease in the Si content was more evident than in the analysis at  $90^\circ$  and confirmed the removal of the most superficial layers due to Ar-implantation. Smaller amounts of Ar were detected in this superficial analysis. The projected range of the implantation profile obtained with the TRIM simulation revealed a lower concentration of the implanted element on the surface sample.

Fig. 5 shows the deconvolution of the in the analysis at  $30^\circ$ . An important decrease of the C–O component was observed with Ar-implantation. It is interesting to observe how the  $1 \times 10^{15}$  Ar $^+$ /cm $^2$  implanted sample presented as much M-OH as M-O on the surface. As a consequence, the increase in the amount of oxygen and iron on the lower implantation dose observed in Fig. 4 was due to the higher contribution of FeOOH and did not necessarily mean an increase in the protective properties of the modified passive layer. However, the hydroxide component tended to decrease with higher implantation doses due to the sputtering explained before. The smaller amount of oxygen detected in higher implantation doses was mainly in form of oxide, providing protection to the modified AISI 304 SS.

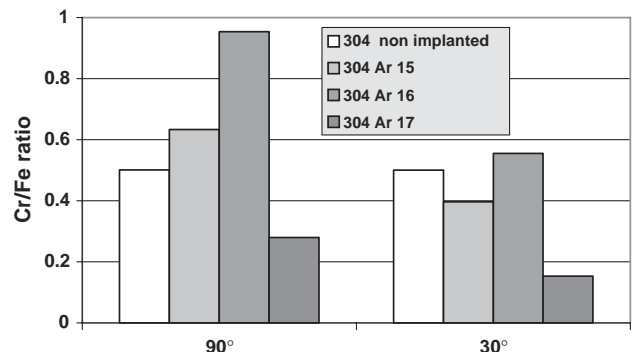


Fig. 6. Comparison of the Cr/Fe ratio at both take off angles.

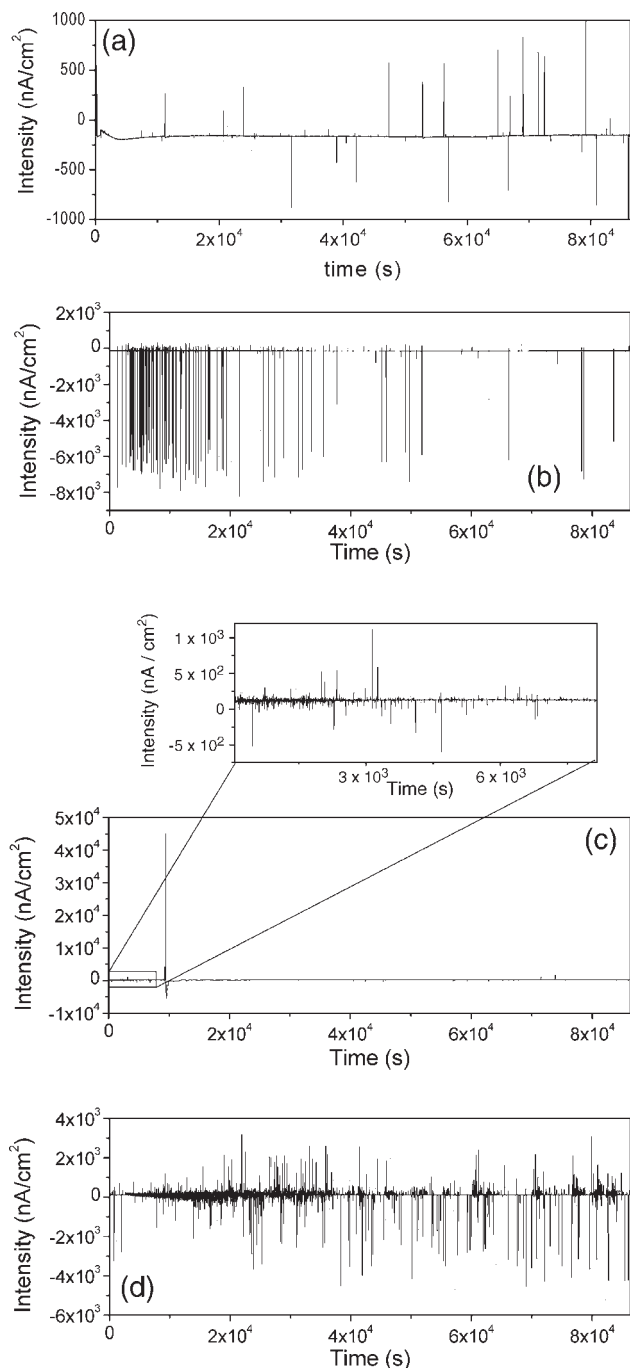


Fig. 7. Intensity vs. time curve in the  $2 \times 10^{-4} \text{ M FeCl}_3$  solution of (a) non-implanted, (b)  $10^{15}$ , (c)  $10^{16}$  and (d)  $10^{17} \text{ Ar}^+/\text{cm}^2$  AISI 304 SS.

As an attempt to determine the protective properties of the implanted surfaces, Fig. 6 shows the evolution of the Cr/Fe ratio with the implantation dose, obtained by comparing the amount of these elements joined with oxygen. The comparison at  $90^\circ$  revealed an increase in the Cr/Fe ratio with the increasing implantation dose due to a Cr enrichment on the passive layer of AISI 304 SS with Ar-implantation. Therefore, better chemical conditions for the corrosion protection were obtained with this treatment in the deeper region of the passive layer. Only the higher implantation dose ( $10^{17} \text{ Ar}^+/\text{cm}^2$ ) presented a drastic reduction of this ratio due to the small amount of Cr detected,

showing the least favourable Cr/Fe ratio. Chang et al. [4] found that a decrease of the Cr and  $\text{Cr(OH)}_3$  peaks was an indication that the typical structure of the sample was broken by ion implantation. O  $1s_{1/2}$  peaks consequently, an important decrease in the protective properties was expected in this sample. On the contrary, Ar-implantation decreased the Cr/Fe ratio on the superficial analysis at  $30^\circ$ , indicating lower protective properties than the deeper analysis in terms of chemical protection. Only the  $1 \times 10^{16} \text{ Ar}^+/\text{cm}^2$  dose increased the Cr/Fe ratio of AISI 304 SS due to its higher Cr content. This sample presented the best composition in terms of corrosion protection.

Noise experiments were performed in order to understand the pit initiation occurrence in Ar-implanted AISI 304 SS. The study of metastable pitting behaviour provides a better understanding of the nucleation mechanism of the localised corrosion processes [22]. With this aim, the samples were first immersed in a 1 M NaCl solution for 24 h. During this period, transients in potential and intensity were only observed in the  $1 \times 10^{17} \text{ Ar}^+/\text{cm}^2$  implanted sample, that revealed the instability of this dose. After this stabilization period, the addition of an oxidising solution such as  $2 \times 10^{-4} \text{ M FeCl}_3$  ensured the apparition of pits due to a significant potential increase. Fig. 7 shows a comparison of the typical current vs. time plots during potentiostatic experiments. This kind of representation shows the transient activity, that is to say, the occurrence of pits through time. The comparison of the current fluctuations revealed an increase in the transient's activity with Ar-implantation. Furthermore, an increase in implantation dose produced an increase in the frequency of pit events. Consequently, Ar-implantation favoured the occurrence of pits in AISI 304 SS.

A  $1 \times 10^{15} \text{ Ar}^+/\text{cm}^2$  dose increased the number of transients at the beginning of the experiments, although the activity as well as the amplitude of these transients tended to decrease with time. The XPS studies revealed an outermost surface mainly composed by  $\text{FeOOH}$ , that explained the increase in the occurrence of pits due to its lower protective properties. However, the better Cr/Fe ratio found in the inner region of the passive layer could be responsible for the decrease in the transients activity at higher immersion times. On the other hand, the  $1 \times 10^{16} \text{ Ar}^+/\text{cm}^2$  implanted sample presented a higher number of transients than the non-implanted and the lower implanted samples at the beginning of the experiments, although a transient with a big response in current and an important decrease in potential hid the presence of transients till the end of the experiment. This case was included so as to show of how a big transient can interfere with the detection of further transients. Therefore, despite the better chemical composition for the corrosion protection found in the XPS analysis, this sample presented an increase in the transients activity of AISI 304 SS and, consequently, a lower corrosion resistance. Finally, the highest implantation dose ( $1 \times 10^{17} \text{ Ar}^+/\text{cm}^2$ ) showed the most important increase in the nucleation frequency of pits as well as in the amplitude of the transients throughout the experiment and both factors increased with the immersion time (in opposition to the lower implanted sample). Therefore, the highest implanted sample produced the biggest decrease in the protective properties of AISI 304 SS. It must be

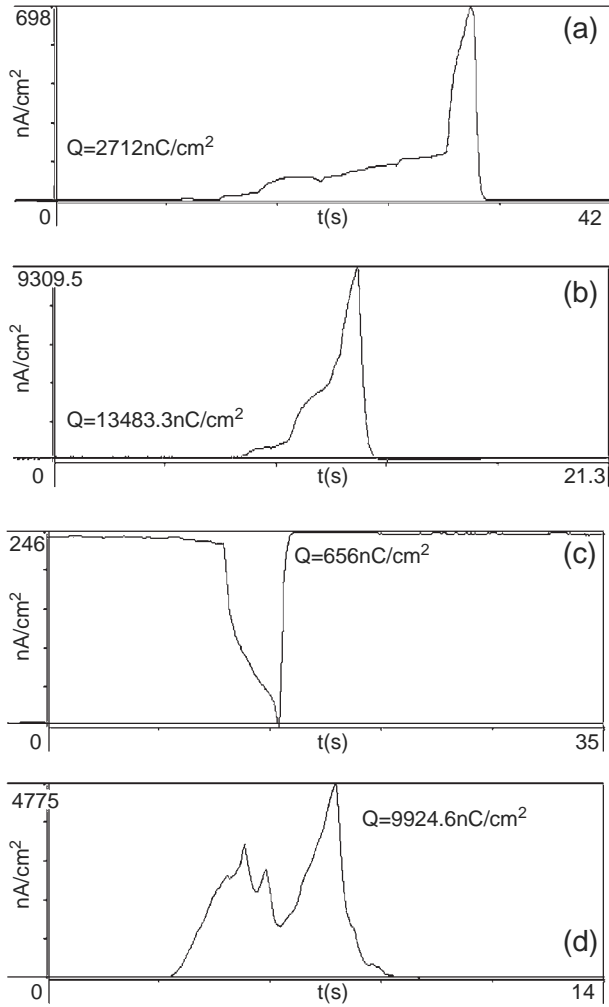


Fig. 8. Typical morphology of the transients found on (a) non-implanted, (b)  $10^{15}$ , (c)  $10^{16}$  and (d)  $10^{17}$   $\text{Ar}^+/\text{cm}^2$  AISI 304 SS.

borne in mind that this was the only sample that registered transients during the first 24 h in the NaCl solution, that revealed the instability of the surface. Furthermore, the XPS analysis showed an important decrease in the Cr content in the passive layer that implied lower corrosion protection as confirmed the noise experiments.

Apart from the nucleation events, Ar-implantation also promoted an increase in the amplitude (height) of the transients. This increase reflected the higher corrosion intensity related to a bigger amount of metal dissolved [23]. Furthermore, the time for repassivation was also modified. In the case of the lower implantation dose ( $10^{15}$   $\text{Ar}^+/\text{cm}^2$ ), the average lifetime of the transients decreased from the 5.5 s of the non-implanted sample to the 3.8 s. However, in the case of higher implantation doses ( $10^{16}$   $\text{Ar}^+/\text{cm}^2$  and  $10^{17}$   $\text{Ar}^+/\text{cm}^2$ ) an increase of the lifetime was found. Both parameters of a pit-amplitude and lifetime-leads to calculate the area of each transient. The parameter obtained with this calculation is the charge associated to each transient. The average charge associated to each transient increases with Ar-implantation from 91  $\text{nC}/\text{cm}^2$  in the non-implanted SS to 463  $\text{nC}/\text{cm}^2$  in the

lower implantation dose, 1924  $\text{nC}/\text{cm}^2$  in the  $1 \times 10^{16}$  ions/ $\text{cm}^2$  or 2734  $\text{nC}/\text{cm}^2$  in the highest implanted sample. The increase in the charge associated to each transient was related to the one magnitude order increase observed in the amplitude of the transients after Ar-implantation that revealed an important mass loss. As a consequence, once a pit is initiated, metal dissolution occurred very fast on Ar-implanted AISI 304 SS. The only aspect that favoured the implanted samples was the logarithmic growth tendency of the number of accumulated pits with time, in contrast to the linear growth of the non-implanted SS. That is to say, an extrapolation of these results for longer periods may result in a decrease in the transient's activity of the implanted specimens below the non-implanted SS. The reason for this behaviour could be partially found on the Cr/Fe ratio of Fig. 6. The Ar-implanted samples presented less favourable ratios on the outer region of the passive layer, leading a higher occurrence of pits. However, the inner region of the passive layer presented a better Cr/Fe ratio than AISI 304 SS. Therefore, if this region was exposed to the aggressive medium, a better performance than the non-implanted sample would have been expected.

Apart from the transient's activity, the morphology of the transients also provide important information about the repassivation ability. Gabrielle et al. [24] described different shapes of the transients. Type I is characterised by a slow increase in intensity followed by a quick decrease, whereas type II is characterised by a quick increase in intensity followed by a slow decrease. The transients shown in Fig. 8 are examples of the predominant transients morphology found in each sample. All of them mainly presented a type I morphology typical of stainless steels [24]. It corresponds to a first approximation of the growth law:  $I(t) \propto t^n$ , where the intensity is proportional to time and the final shape of the transients depends on the  $n$  value. When  $n < 1$ , the transient is considered type Ia characterised by a plateau and a fast increase in intensity, followed by a quick decrease of the cathodic current. When  $n > 1$ , the transient is considered type Ib and presented a steady increase in current followed by a fast repassivation [25]. Fig. 8a shows the typical Ia morphology predominantly found on the non-implanted AISI 304 SS. Ar-implantation modified the shape of the transients. The  $1 \times 10^{15}$   $\text{Ar}^+/\text{cm}^2$  implanted sample also presented a predominant Ia morphology (Fig. 8b), although reducing the length of the plateau observed in the non-implanted sample and, consequently, the lifetime of the pit. However, the amplitude as well as the charge associated is increased and a higher metal dissolution took place in a shorter period. Higher implantation doses revealed a modification on the shape of the transients. The  $1 \times 10^{16}$   $\text{Ar}^+/\text{cm}^2$  implanted sample (Fig. 8c) reduced even more the length of the plateau and the shape of the transients is closer to a type Ib. Finally, the highest implantation dose ( $10^{17}$   $\text{Ar}^+/\text{cm}^2$ ) predominantly showed very complex transients like the one shown in Fig. 8d. This kind of transients could not be included in previous described morphologies due to its complexity. The oscillations on the intensity reflects the difficulty for repassivation of this sample. Therefore, Ar-implantation not only modifies the frequency of appearance of pits but also the

transients morphology, showing a different metastable pitting behaviour.

In addition to the physical modifications, the XPS analysis confirmed that Ar-implantation modified the surface composition of AISI 304 SS. Both factors explained the modification observed on the pitting behaviour. Ar-implantation decreased the Cr/Fe ratio on the outer region of the passive layer, decreasing the chemical conditions for protection of AISI 304 SS. However, the XPS analysis of an inner region of the passive film showed an increase of the Cr/Fe ratio with Ar-implantation and a more favourable composition in terms of corrosion protection. Beside this fact, it must be taken into account that the higher damaged region was located on the outer part of the surface. As a consequence, when a dissolution process took place, a region with better protective properties and smaller number of defects was reached, favouring the repassivation process as showed the fast decrease in current found on the transients (Fig. 8) of the implanted samples. The only exception was once again the highest implantation dose, that presented an important decrease in the Cr content on the passive layer, decreasing its protective properties, apart from the higher radiation damage due to the higher fluence employed. The strong residual stresses generated by the implanted Ar in the passive film could contributed to the breakdown phenomenon [26].

Certain similarities have been found between ion implanted stainless steels and cold worked stainless steels [19]. A decrease in the pitting resistance in cold worked stainless steel was attributed to the high density of defects produced by deformation and to the defective passive film developed [27]. Therefore, the pitting corrosion resistance is also conditioned in a greater extent by the physical modifications. The damage induced on the surface of the stainless steel due to Ar-implantation generated a decrease in the protective properties as revealed the noise experiments. Therefore, once a pit was initiated, it propagated very fast as the measured amplitude was higher than the non-implanted material. The faster propagation rate was related to the higher number of defects on the surface. Regions with a high dislocation density could be considered as high stressed regions and, hence, they can act as potential pitting sites [27]. Consequently, the increase in the transient's activity could be related to the parallel increase in the dislocation density and the damage produced. Furthermore, the highest implantation dose ( $10^{17} \text{ Ar}^+/\text{cm}^2$ ) increased the amplitude of the transients with time, in contrast with the decrease found in the lower implanted sample ( $10^{15} \text{ Ar}^+/\text{cm}^2$ ). This fact revealed an increase in the activity of the surface with time highest. Different corrosion tests performed on Ar-implanted AISI 304 SS [13] revealed an improvement of the corrosion behaviour as the immersion time increased and must be object of further analysis in the future.

#### 4. Conclusions

- Argon implantation modifies the composition of the passive layer of AISI 304 SS. It decreases the Cr/Fe ratio in the outer region of the passive layer and promotes a less protective surface in terms of composition. However, there

is an increase in this ratio in the inner region of the passive layer.

- $1 \times 10^{16} \text{ Ar}^+/\text{cm}^2$  is a threshold fluence to generate a thinner passive layer due to sputtering.
- Ar-implantation modifies the metastable pitting behaviour of AISI 304 SS. It increases the surface activity, the appearance of metastable pits, the amplitude and the charge associated to each transient. This behaviour increases with the implantation dose.
- Ar-implantation modifies the transients morphology, increasing its complexity, and hindering any attempt to establish the mechanism of pit initiation of the modified material.
- The  $1 \times 10^{15} \text{ Ar}^+/\text{cm}^2$  dose presents a smaller transient activity than higher doses despite the less protective FeOOH of its surface. The physical modifications induced have an important role on the generation of pitting potential sites after Ar-implantation.
- The  $1 \times 10^{17} \text{ Ar}^+/\text{cm}^2$  dose generates the most important decrease in the protective properties of AISI 304 SS. The low Cr content on the passive layer and the highly damaged surface produces the highest transient's activity and a complex morphology of the transients.

#### References

- [1] M. Seo, N. Sato, *Trans. Jpn. Inst. Met.* 21 (1980) 805.
- [2] P.Q. Zhang, J.X. Wu, Q. Zhang, X.Y. Lu, K. Wang, *Corros. Sci.* 34 (1993) 1343.
- [3] C. Blawert, H. Kalvelage, B.L. Mordike, G.A. Collins, K.T. Short, Y. Jirásková, O. Schneeweiss, *Surf. Coat. Technol.* 163 (2001) 181.
- [4] G.S. Chang, J.H. Son, S.H. Kim, K.H. Chae, C.N. Whang, E. Menthe, K.-T. Rie, Y.P. Lee, *Surf. Coat. Technol.* 112 (1999) 291.
- [5] E. Leitaio, R.A. Silva, M.A. Barbosa, *J. Mater. Sci., Mater. Med.* 8 (1997) 365.
- [6] J. Mater. Sci., *Mater. Med.* 8 (1997) 365.
- [7] H. Ferber, G.K. Wolf, *Mater. Sci. Eng.* 90 (1987) 213.
- [8] R. Devaux, D. Vouagner, A.M. Becdelievre, C. Duret-Thual, *Corros. Sci.* 36 (1994) 171.
- [9] R. Sabot, R. Devaux, A.M. de Becdelievre, C. Duret-Thual, *Corros. Sci.* 33 (7) (1992) 1121.
- [10] W.J. Ensinger, in: Y. Pauleau, P.B. Barna (Eds.), *Protective Coatings and Thin Films*, vol. 585, 1997.
- [11] F. Noli, P. Misaelides, H. Baumann, A. Hatzdimitriou, *Corros. Sci.* 38 (1996) 2235.
- [12] S. Virtanten, Y. Kobayashi, H. Böhni, *Proc.- Electrochem. Soc.* 17 (1998) 281.
- [13] F.J. Pérez, M.P. Hierro, C. Gómez, L. Martínez, P.G. Viguri, *Surf. Coat. Technol.* 155 (2002) 250.
- [14] J.F. Ziegler, J.P. Biersack, *The Stopping and Range of Ions in Solids*, Pergamon Press, New York, ISBN-0-08-021603-X, 1985.
- [15] Thesis "Etude d'une nouvelle methode électrochimique de mesure de la corrosion localisée au potentiel d'abandon" Grégory Berthomé, LTPCM-INPG Grenoble, September 17th 2002.
- [16] A. SadoughVanini, J.P. Audouard, P. Marcus, *Corros. Sci.* 36 (1994) 1825.
- [17] P.L.F. Hemment, *Vacuum* 29 (1979) 439.
- [18] M. Terasawa, T. Mitamura, L. Liu, H. Tsubakino, M. Niibe, *Nucl. Instrum. Methods Phys. Res., B Beam Interact. Mater. Atoms* 193 (2002) 329.
- [19] N. Mottu, M. Vayer, R. Erre, *Surf. Coat. Tech.* 183 (2004) 165.
- [20] L. Wegrelius, F. Falkenberg, I. Olefjord, *J. Electrochem. Soc.* 146 (1999) 1397.
- [21] Hong-Hua Ge, Guo-Ding Zhou, Wen-Quan Wu, *Appl. Surf. Sci.* 211 (2003) 321.

- [22] Yu Zuo, Haiou Du, Jinping Xiong, J. Mater. Sci. Technol. 16 (2000) 286.
- [23] Darja Kek Merl, Peter Penjan, Milha Čekada, Marijan Maček, Electrochim. Acta 49 (2004) 1527.
- [24] C. Gabrielle, F. Huet, M. Keddam, Proceedings of the 2nd International Conference on Localised Corrosion, Orlando, 1997, p. 93.
- [25] Thesis “Mesures de bruit par piqûration sur des alliages fer-chrôme” Claire Boulleret. Université de Paris XI, September 18th 1997.
- [26] U. Kamachi Mudali, Electrochim. Acta 46 (2001) 3735.
- [27] U. Kamachi Mudali, P. Shankar, S. Ningshen, R.K. Dayal, H.S. Khatak, Baldev Raj, Corros. Sci. 44 (2002) 2183.